THE ASTROPHYSICAL JOURNAL, 238:1126–1133, 1980 June 15

THERMAL MODELS FOR SOLAR HARD X-RAY BURSTS

DEAN F. SMITH
Department of Astro-Geophysics, University of Colorado at Boulder
AND
LAWRENCE H. AUER
High Altitude Observatory, National Center for Atmospheric Research,[1] Boulder, Colorado
Received 1979 October 4; accepted 1979 December 12

ABSTRACT

Thermal models for hard X-ray bursts consisting of a one-dimensional flux tube whose central electrons are heated to $\sim 4 \times 10^8$ K are examined using a numerical scheme which can handle steep gradients without introducing artificial diffusion. In addition to classical thermal conductivity, a heat flux limit is applied to handle the cases of saturated and instability-limited thermal conduction. The enhanced electron-ion thermal coupling caused by ion-acoustic waves is also included and turns out to influence strongly the source development. When this coupling is weak in the sense that electron losses to ions are compensated by additional heating and only tail ions gain energy, the ion-acoustic instability strongly limits the heat flux and the source bifurcates into two regions of different temperature, a process which leads to a power-law X-ray spectrum. When this coupling is strong in the sense that the bulk of the ions is heated, a case which does not occur in simulations and experiments, the ion-acoustic instability limits the heat flux weakly and the source is dominated by a single temperature region which leads to a thermal X-ray spectrum.

Subject headings: hydromagnetics — Sun: corona — Sun: X-rays — X-rays: bursts

I. INTRODUCTION

In a previous paper (Smith and Lilliequist 1979, hereafter SL) we investigated both analytically and numerically the one-dimensional evolution of a flux tube with electrons heated to $\sim 4 \times 10^8$ K. An analytical treatment of this problem was also given by Brown, Melrose, and Spicer (1979, hereafter BMS). Arguments for the importance of this problem in understanding flare energetics and constraints on the electron acceleration or energization process are given in BMS and SL. Emslie and Brown (1980) have shown that a thermal source leads to hard X-ray polarization and directivity compatible with the most recent observations (Tindo, Shuryghin, and Steffen 1976). Recent analysis of two impulsive simultaneous microwave and hard X-ray bursts by Wiehl and Schöchlin (1980) show that they fit a thermal model of the type postulated in SL and BMS. Finally, Smith (1980) has shown that with present models for the primary energy release in solar flares, at most 0.1% of the flare energy is deposited into nonthermal streaming electrons of the energy required in thick-target hard X-ray burst models, and thus present models for the primary energy release are compatible only with thermal hard X-ray burst models.

While the analysis in SL did lead to basically correct results, as we shall see from the much more complete analysis of this paper, it suffered from the following defects: (1) The numerical scheme used required the use of an artificial thermal conductivity which obscured some of the more detailed physics of the process. (2) The effect of ion-acoustic waves in enhanced electron-ion thermal coupling due to the presence of ion-acoustic waves was not taken into account explicitly although the use of an artificial thermal conductivity in many ways mimicked this effect. Here we use a numerical scheme which requires no artificial heat conduction and allows us to follow accurately the thermal evolution of electrons and ions. Like SL, only one equation of motion is employed which follows the center of mass motion of electrons and ions.

Runs were made with no enhanced electron-ion thermal coupling (hereafter the weak coupling case) and with the enhanced electron-ion thermal coupling of Manheimer (1977; hereafter the strong coupling case). The magnitude of this coupling turned out to be a crucial factor in determining the heat containment and thus the X-ray spectrum. In the case of weak coupling, the heated electrons separate into a region of high temperature $\sim 4 \times 10^8$ K and a region of lower temperature $\sim 10^8$ K, a process which leads to a power-law X-ray spectrum as often observed. In the case of strong coupling this phenomenon does not occur and the evolution is similar to a classical conduction front (Zeldovich and Raizer 1967). There is only one dominant temperature, $\sim 2 \times 10^8$ K, and the X-ray spectrum resembles a true thermal spectrum

[1] The National Center for Atmospheric Research is supported by the National Science Foundation.

which is the other type of spectrum commonly observed.

In § II we present the physical details and basic equations of the problem. Numerical methods which allow the accurate solution of these equations and specific forms for some terms are given in § III. Results are presented in § IV, and implications of the results and suggestions for further research are discussed in § V.

II. PHYSICAL BACKGROUND

As in SL we consider a flux tube with energy deposited into electrons near the center and apply symmetric boundary conditions at this point, hereafter the origin. As a result, heat is conducted away from this point. The rate of heating is sufficient to heat the electrons near the origin to $\sim 4 \times 10^8$ K in a few seconds. As discussed in SL, in addition to classical heat conduction, conduction can become saturated corresponding to direct convection by electrons which leads to a heat flux,

$$Q_{\rm SAT} = \tfrac{1}{4} n m_e v_e^3 , \tag{1}$$

where n is the electron or ion density, $v_e = (KT_e/m_e)^{1/2}$ is the electron thermal velocity, and T_e is the electron temperature. Heat conduction can also be anomalously limited as in Manheimer (1977) due to ion-acoustic instability of the return current which compensates the forward current formed by the heat-carrying electrons. The heat flux in this case is

$$Q_{\rm AN} = \tfrac{3}{2} n K T_e \left\{ \left[\frac{K(T_e + 3T_i)}{m_i} \right]^{1/2} + \left(\frac{m_i}{m_e} \right)^{1/2} \left(\frac{T_e}{T_i} \right)^{3/2} \frac{K^{1/2}}{m_i^{1/2}} (T_e + 3T_i)^{1/2} \times \exp\left(- \frac{0.5 T_e/T_i + 1.5}{1.25} \right) \right\} , \tag{2}$$

where T_i is the ion temperature. The complex behavior of $Q_{\rm AN}$ as a function of T_e/T_i, which is discussed in § III, is the primary cause of the complex thermal source structure we shall find in § IV*b*. The physical cause of this behavior is the following. The second term in brackets in equation (2) represents Landau damping of ion-acoustic waves by ions. As T_e/T_i increases from 10 to 20, this damping rapidly turns off, which allows the ion-acoustic waves to grow to larger amplitudes and thus limit the heat flux more effectively.

The calculations discussed in § IV include all of the above possibilities for the heat flux and also the enhanced electron cooling and ion heating due to the presence of ion-acoustic waves. Since this is a new aspect not included in SL which significantly affects the results, we consider it in some detail. The hydrodynamic equations which describe the evolution of our system are

$$\frac{\partial n}{\partial t} + \frac{\partial}{\partial x} n v = 0 , \tag{3}$$

$$n m_i \frac{\partial v}{\partial t} + n m_i v \frac{\partial v}{\partial x} + \frac{\partial}{\partial x} n K (T_e + T_i) = 0 , \tag{4}$$

$$\frac{3}{2} \frac{\partial}{\partial t} n K T_e + \frac{3}{2} \frac{\partial}{\partial x} n K T_e v + n K T_e \frac{\partial v}{\partial x} + \frac{\partial Q}{\partial x} = C_{\rm te} - \tfrac{3}{2} n K (T_e - T_i) f_{\rm eq} + \frac{\partial \epsilon}{\partial t} + R_L , \tag{5}$$

$$\frac{3}{2} \frac{\partial}{\partial t} n K T_i + \frac{3}{2} \frac{\partial}{\partial x} n K T_i v + n K T_i \frac{\partial v}{\partial x} = C_{\rm ti} + \tfrac{3}{2} n K (T_e - T_i) f_{\rm eq} , \tag{6}$$

where v is the center of mass velocity of electrons and ions, Q is the electron heat flux, $f_{\rm eq}$ is the classical electron-ion equipartition rate, $\partial\epsilon/\partial t$ is the energy source term, and R_L is the radiative loss rate which was taken in the same form as SL. The terms $C_{\rm te}$ and $C_{\rm ti}$ are the electron cooling and ion heating rates due to the ion-acoustic instability which are given by (Manheimer 1977)

$$C_{\rm te} \approx - \frac{\pi c_s |k| Q}{2(2\pi)^{1/2} v_e^5} \left[\frac{e\phi(k)}{m_e} \right]^2 , \tag{7}$$

and

$$C_{\rm ti} \approx - C_{\rm te} . \tag{8}$$

Here $c_s \approx (KT_e/m_i)^{1/2}$ is the sound speed, k is the wavenumber of the ion-acoustic wave, and $\phi(k)$ is the fluctuation level of the ion-acoustic waves. Following Manheimer (1977) we set $\phi(k) = \phi_0 \delta(k - k_D/2)$, where $k_D = \omega_{\rm pe}/v_e$ is the Debye wavenumber, and $\omega_{\rm pe}$ is the electron plasma frequency.

A term $n\omega/v_e^3$ which would reduce the right-hand side of equation (7) somewhat has been dropped, which makes equation (7) a conservative upper limit. Here ω is the angular frequency of the ion-acoustic waves. The reason for using an overestimate of $C_{\rm te}$ is the following: To obtain most of the terms in equations (3)–(6) Manheimer (1977) uses a slightly modified drifting Maxwellian electron distribution and a Maxwellian ion distribution. The electron distribution is consistent with experiment, but the ion distribution is not as noted by Manheimer (1977). Both simulations (Caponi and Krall 1975) and experiment (Stenzel and Gekelman 1978) show that in the presence of ion-acoustic waves the bulk of the ions are not heated. Rather, a hot ion tail forms on the ion distribution. As suggested by Manheimer (1977), to model this effect properly would require at least one more fluid equation than equations (3)–(6). Our approach has been to use equations (3)–(6) and bracket the possible results of an analysis using more equations by either setting $C_{\rm te} = C_{\rm ti} = 0$ (weak coupling) or giving them the values of equations (7)–(8) (strong coupling) which are conservative upper limits. We call these cases weak and strong electron-ion coupling, respectively, because the

finite C_{te} and C_{ti} terms have exactly the same physical effect as enhancing the electron-ion equipartition rate f_{eq}.

III. NUMERICAL METHOD

There are two basic problems which arise in solving equations (3)–(6). First, when the heat flux becomes saturated (eq. [1]), Q is not proportional to the gradient of T_e which changes the character of the energy equation from parabolic to hyperbolic. The method of solution must be able to handle this change. Second, because of the presence of strong shocklike structures in the solutions, the method must be stable in the presence of strong gradients. To overcome these problems we have developed a hybrid version of the flux-corrected transport algorithm (Boris and Book 1976) in which the convective parts of the equations are treated explicitly and the diffusion parts implicitly. Details of this scheme are given in the Appendix.

The transitions between classical, saturated, and anomalously limited heat fluxes are handled by the empirical procedure of Zimmerman (1978, private communication) as in laser fusion codes, i.e.,

$$Q = \frac{(3/2)nKT_e v_e}{\alpha n \ln \Lambda / T_e + R(T_e/T_i)(dT_e/dx)} \frac{dT_e}{dx}, \quad (9)$$

where $\alpha = 4.37 \times 10^{-6}$ and $\ln \Lambda$ is the Coulomb logarithm. In the limit of low electron temperature and/or temperature gradient, we recover the classical conductive flux Q_{CL}. In the high gradient limit, the flux is a function only of the electron and ion temperatures and density. The function

$$R(T_e/T_i) = 2 + 6Q_{SAT}/Q_{AN}, \quad (10)$$

which is plotted in Figure 1, measures the degree to which the free streaming of electrons is restricted by saturation and/or ion-acoustic waves. The constants in equation (10) were chosen such that Q_{SAT} is recovered when $T_e \approx T_i$, and Q_{AN} is recovered when $T_e \approx 10T_i$.

IV. RESULTS

The physical problem studied is the same as in SL, but the study was done with much more complete parameter variations and diagnostics. We consider a 10,000 km long flux tube which can be thought of as an arch with electron heating near the top. By symmetry only one-half of the arch needs to be considered, and x measures distance from the center of the arch. For the left boundary at $x = 0$, the boundary condition was

$$v = 0; \quad \frac{\partial T_e}{\partial x} = \frac{\partial T_i}{\partial x} = 0.$$

For the right boundary at $x = 5000$ km, the boundary condition was

$$\frac{\partial^2 v}{\partial x^2} = \frac{\partial^2 T_e}{\partial x^2} = \frac{\partial^2 T_i}{\partial x^2} = 0.$$

The right boundary condition corresponds to a free boundary. The energy input is of the form

$$\frac{\partial \epsilon}{\partial t} = \frac{F(t)}{(2\pi)^{1/2}\sigma} \exp\left(\frac{-x^2}{2\sigma^2}\right),$$

where

$$F(t) = tS, \quad t < 0.75 \text{ s},$$
$$F(t) = S, \quad t \geq 0.75 \text{ s},$$

$\sigma = 500$ km, and S is varied to correspond to average energy inputs of $1\text{–}8 \times 10^4$ ergs cm^{-3} s^{-1} over 500 km.

The initial temperatures were $T_e = T_i = 10^6$ K, and the initial velocity was zero. Both uniform and exponentially increasing initial density profiles were used. Most of the runs were made with a uniform initial density of $n = 3 \times 10^{11}$ cm^{-3}, which can be assumed unless otherwise stated.

This section is divided into three subsections. In § IV*a* we attempt to understand the effect of the variation of the function R (eq. [10]) on the results by setting $R = 6$, which is its lowest value (cf. Fig. 1), corresponding to saturated heat flux only. In §§ IV*b* and IV*c* both saturated and anomalously limited heat flux are considered in the weak and strong electron-ion coupling cases, respectively.

a) Results with Saturated Heat Flux Only and Weak Electron-Ion Coupling

The main reason for running this case was to show that saturated heat flux alone could not produce the two-temperature behavior characteristic of § IV*b*. The results are qualitatively the same as Figure 6 except that the steep gradient in T_e, the conduction front, reaches the same point as in Figure 6 at 1.4 s when the maximum T_e is about 2×10^8 K with the same energy input of 6×10^4 ergs cm^{-3} s^{-1}. The conduction front moves at a larger speed than in Figure 6 because there is no additional inhibition of conduction due to ion-acoustic waves. The absence of a two-temperature structure in this case shows that this characteristic of the next subsection is due to the rapid variation in R in the range $10 \leq T_e/T_i \leq 20$ shown in Figure 1 and not to the weak electron-ion coupling.

b) Results with Saturated and Anomalously Limited Heat Flux with Weak Electron-Ion Coupling

We progress now to the case where the heat flux may be limited by saturation and further limited by ion-acoustic instability as shown in Figure 1. However, the C_{te} and C_{ti} terms (eqs. [7]–[8]) are set equal to zero as a limiting case for the reasons given in § II. Physically, this case would arise if there were additional Joule dissipation of a current to compensate the electron cooling and the number of ions in the hot ion tail created were sufficiently small to have no effect. Results for this case are shown in Figures 2–5.

Analysis of these results leads to the following observations. For energy inputs less than or equal to

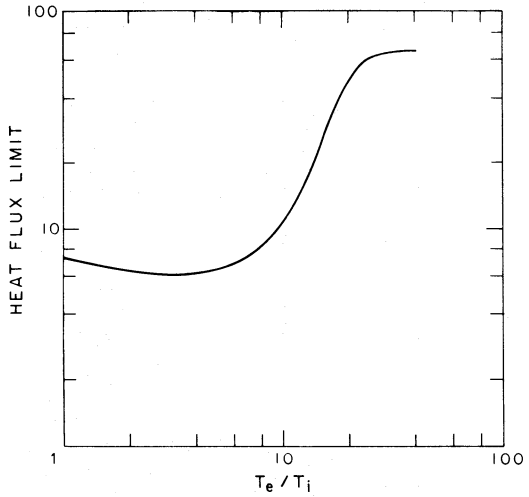

FIG. 1.—The heat flux limiting function R of eq. (10) as a function of T_e/T_i.

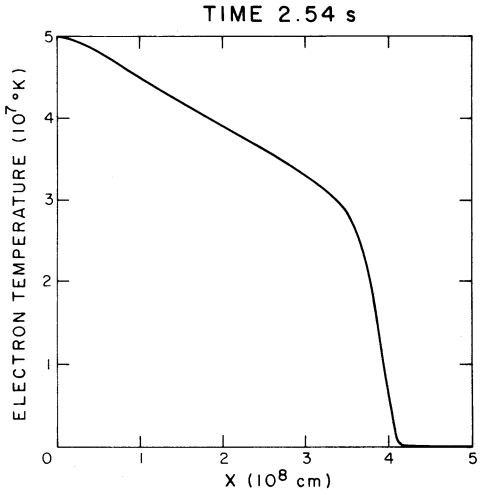

FIG. 2.—The electron temperature along the flux tube for an energy input of 10^4 ergs cm^{-3} s^{-1} and weak electron-ion thermal coupling.

10^4 ergs cm^{-3} s^{-1} the behavior is like a classical conduction front as shown in Figure 2, and anomalously limited conduction plays no role. For energy inputs greater than or equal to 2×10^4 ergs cm^{-3} s^{-1} a dramatic change occurs as shown in Figure 3*a*. A two-electron temperature regime becomes pronounced after about 1 s and persists thereafter unlike any classical result. The velocity shown in Figure 3*b* has a much rougher plateau at about 500 km s^{-1} in the same region as the 86 million degree T_e quasi-plateau. The whole flux tube is in approximate pressure equilibrium out to $x = 4000$ km, where $n = 4.3 \times 10^{11}$ cm^{-3}. At $x = 100$ km, $n = 8.8 \times 10^{10}$ cm^{-3} which shows that the density hole produced by the electron heating is much more pronounced than in SL. The approximate pressure equilibrium is a result of the fact that all velocities are subsonic behind the first steep T_e rise in Figure 3*a* which we shall hereafter call the right conduction front. The ion-acoustic speed in the 86 million degree plasma is 8.5×10^7 cm s^{-1}.

Figure 4 shows the temperature profiles for an energy input of 6×10^4 ergs cm^{-3} s^{-1}. It should be noted that although the temperature of the quasi plateau behind the right conduction front in this case has risen to 120×10^6 K, the leading edge of the right conduction front is in the same place as in Figure 3*a*, in contradiction to the surmise of BMS and SL that the conduction front moves at the ion-acoustic speed of

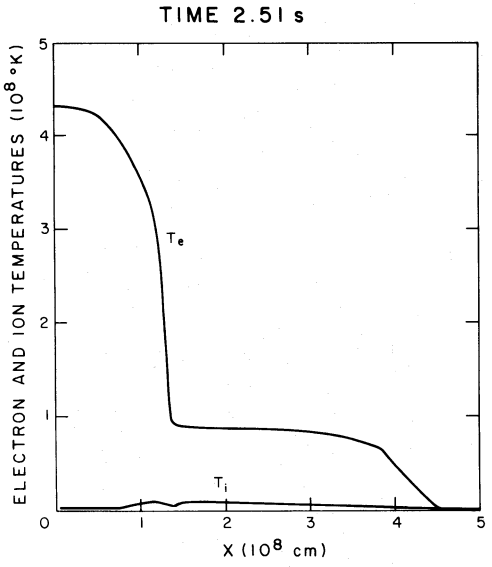

FIG. 3*a*

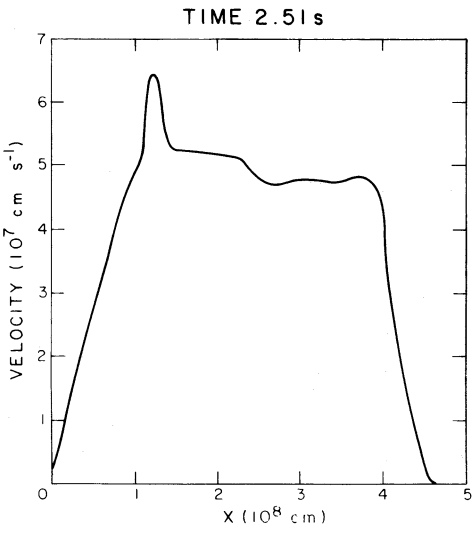

FIG. 3*b*

FIG. 3.—(*a*) Electron and ion temperatures along the flux tube for an energy input of 3×10^4 ergs cm^{-3} s^{-1} and weak electron-ion coupling. (*b*) Velocity along the flux tube for the same conditions as (*a*).

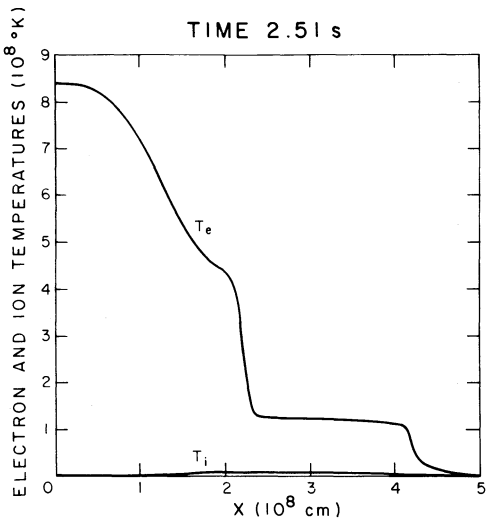

FIG. 4.—As for Fig. 3*a* with an energy input of 6×10^4 ergs cm^{-3} s^{-1}.

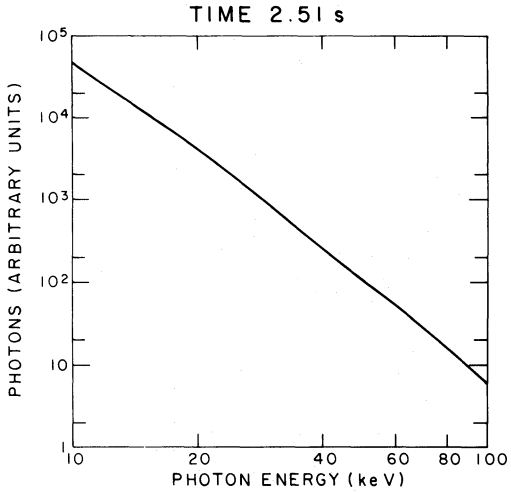

FIG. 5.—The photon spectrum for the case of Fig. 3*a*

the hot electrons behind the front. This constancy of propagation speed of the right front was observed for energy inputs from 2 to 8×10^4 ergs cm^{-3} s^{-1}. Changing the initial temperatures to $T_e = T_i = 1.5 \times 10^6$ K showed the same constancy, but with a slightly higher propagation speed which clearly indicated that this speed depended on the upstream rather than the downstream temperature. A careful investigation of the properties of the heat-flux limitation revealed the source of this behavior. In the right conduction front $10 \leq T_e/T_i \leq 20$ and the heat flux is being strongly anomalously limited, as shown in Figure 1. The functional T_e dependence of this limitation in the range $10 \leq T_e/T_i \leq 20$ is such that the heat flux $Q \propto T_e^{-\alpha}$, where $\alpha \approx 0.5$. The physical implications of this dependence of Q can be seen by writing $Q = C_1 T_e^{-\alpha}$ and inserting it in the simplest form of equation (5),

$$C_2 \frac{\partial T_e}{\partial t} = -\frac{\partial Q}{\partial x} = \alpha C_1 T_e^{-\alpha-1} \frac{\partial T_e}{\partial x}, \qquad (11)$$

where C_1 and C_2 are constants. Equation (11) is of the form

$$\frac{\partial T_e}{\partial t} = v_c \frac{\partial T_e}{\partial x}, \qquad (12)$$

which has the solution $v_c = \partial x/\partial t$, implying that v_c is the characteristic propagation velocity. Comparison of equations (11) and (12) shows that $v_c \propto T_e^{-\alpha-1}$, which implies for $\alpha > -1$ that v_c is determined by the lowest electron temperature in the problem, the upstream temperature. Since with $\alpha \approx 0.5$ we are strongly into this regime, the physical basis of our result is clear.

The left conduction front dividing the 4×10^8 K electrons from the 86×10^6 K electrons in Figure 3*a* is dominated by convection, a fact which explains why its position in Figure 4 has changed relative to Figure 3*a*. The velocity in the quasi-plateau region for an energy input of 6×10^4 ergs cm^{-3} s^{-1} is 840 km s^{-1}, as compared to 500 km s^{-1} for an energy input of 3×10^4 ergs cm^{-3} s^{-1}, a fact which explains the relative positions of the left conduction fronts in Figures 3*a* and 4. Another diagnostic printed out is the ratio of the actual heat flux to the classical heat flux which would have been carried in the absence of anomalous limitation. This ratio reached values as low as 10^{-4} in back of both of the conduction fronts of Figure 3*a* and stayed less than 10^{-1} over most of the plateau in back of the right front. Since this ratio is directly related to the level of ion-acoustic waves excited by the return current, its low value over extended regions implies that waves are excited over these regions and not confined to thin fronts.

The bremsstrahlung spectrum for the case of Figure 3 is shown in Figure 5. The spectrum is a power law to a good approximation of the form $\epsilon^{-\gamma}$, where ϵ is the photon energy and $\gamma = 3.9$. It is well known that any spectrum can be synthesized by a suitable distribution of thermal sources (Brown 1974). In our case the two temperature regimes give contributions which result in a power law with an index in the range of observed spectral indices (Kane 1974) for times from 1.5 to 2.5 s. As might be expected, varying the energy input changes the spectrum; e.g., the spectral index for Figure 4 with a doubled energy input is 3.5, while the spectral index for an energy input of 2×10^4 ergs cm^{-3} s^{-1} is 5.0. We have made no attempt to reproduce the entire range of observed spectral indices (2–6) since loss processes not included in the models studied are probably also important. The deviations from a power law are well within experimental uncertainties for this commonly observed type of hard X-ray spectrum (see Fig. 22 of Hoyng, Brown, and van Beek 1976).

Finally, some runs were made with an exponentially increasing density of the form $n_0 \exp(x/H)$, with a scale height H of 5000 km. This had the effect of (1)

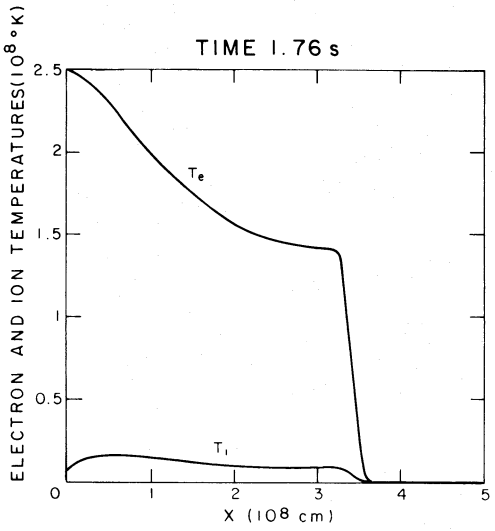

FIG. 6.—Electron and ion temperatures along the flux tube for an energy input of 6×10^{12} ergs cm^{-3} s^{-1} and strong electron-ion coupling.

accelerating the initial development of a two-temperature regime for small x since the amount of energy per electron per unit time put in was relatively greater and (2) retarding the development for larger x. The general results remained unchanged. It should be noted that observations of compact loops are consistent with pressure equilibrium throughout the loop (Jordan 1975) and thus an initially uniform density is consistent with an initially uniform temperature.

c) *Results with Saturated and Anomalously Limited Heat Flux with Strong Electron-Ion Coupling*

We consider the case where the C_{te} and C_{ti} terms in equations (5)–(6) have the values given by equations (7)–(8). In this case, which is an opposite limiting case to that of § IV*b*, the bulk of the ions are heated, contrary to both simulation and experiment. Thus its main interest is as a limiting case which can be considered with only one ion temperature equation. The result for an energy input of 6×10^4 ergs cm^{-3} s^{-1} is shown in Figure 6. This result can be compared directly with Figure 4, which has the same initial conditions and energy input. The times are different in the two figures because the heat flux is much more severely limited in Figure 4 than in Figure 6, which results in a slower propagation speed for the conduction front. In general, Figure 6 has the appearance of a classical conduction front (Zeldovich and Raizer 1967) which is characterized approximately by a single temperature $T_e \approx 2 \times 10^8$ K. The bremsstrahlung spectrum of this source varies only slightly from that of a single temperature source with a distinct decrease of photons near 100 keV (see Elcan 1978) and thus is not shown. This thermal spectrum is the other type commonly observed (Crannell *et al.* 1978; Elcan 1978).

Because of a density depression with $n \approx 1.6 \times 10^{11}$ cm^{-3} near $x = 0$ and a density enhancement with $n \approx 4.7 \times 10^{11}$ cm^{-3} near $x = 3.3 \times 10^8$ cm and a smaller T_e variation, the flux tube in this case is not in pressure equilibrium. Conduction is now so effective that source evolution occurs more rapidly than the time scale required for good pressure equilibration.

V. DISCUSSION

We have seen in §§ IV*b* and IV*c* that the evolution of a thermal X-ray source is a sensitive function of the electron-ion thermal coupling and the state of the plasma into which the source expands. It can be argued that case (*b*) is much closer to a realistic case on the following grounds: Case (*b*) would be realistic with a small amount of additional electron heating if the hot ion tail were to have no appreciable effect on the ion-acoustic instability. The main effect of the hot ions is to saturate the instability at the trapping limit where $e\phi_{tr}/KT_e \approx 0.25$, as long as their density is sufficiently low to have a negligible effect on the dispersion properties of the waves. We shall assume that this density requirement is satisfied in the following discussion because the density required to saturate the instability is small (Caponi and Krall 1975). Thus, when the instability is far from the trapping limit, the hot ions have no effect other than to take up the electron energy transferred due to the enhanced electron-ion thermal coupling. The maximum value of $e\phi/KT_e$ found in case (*b*) was 2.2×10^{-3}, more than an order of magnitude below the trapping limit. Hence, case (*b*) is a realistic calculation when a source of additional electron heating is present to balance the loss to hot ions.

In case (*c*) the effect of heating the bulk of the ions on the ion-acoustic instability is more severe because the ratio T_e/T_i directly affects the threshold for instability (Stringer 1964) which is reflected in Figure 1. In case (*c*) T_e/T_i never becomes much larger than 10, and thus the ion-acoustic instability never strongly limits the heat flux. Correspondingly, the maximum value of $e\phi/KT_e = 2.2 \times 10^{-4}$ was an order of magnitude smaller than in case (*b*). As already noted, case (*c*) is far from any possible realistic case because both simulation (Caponi and Krall 1975) and experiment (Stenzel and Gekelman 1978) show that the bulk of the ions is not heated in the current-driven ion-acoustic instability. However, the ratio T_e/T_i can be limited to values not much larger than 10 for the following other reasons: (1) The rate of energy input is low as in Figure 2. (2) There is no additional electron heating to balance the losses to hot ions.

On the basis of our results and the above discussion we come to the following conclusion about the nature of the two commonly observed types of hard X-ray spectra in the context of a thermal model. When the energy input is less than 2×10^4 ergs cm^{-3} s^{-1} and/or there is insufficient additional electron heating to allow T_e/T_i to rise much above 10, the conduction front is similar in nature to a classical front and the spectrum is

thermal. When the energy input is $\gtrsim 2 \times 10^4$ ergs cm^{-3} s^{-1} and there is sufficient additional electron heating to allow T_e/T_i to rise much above 10, the conduction front bifurcates into two fronts as a result of strong heat-flux limitation by the ion-acoustic instability and the spectrum is a power law during most of the life of the source.

Since we have computed the spectrum (Fig. 5), a much better calculation of the gain in efficiency compared to a nonthermal streaming model is possible than the estimate in SL. The spectrum of Figure 5 has an index $\gamma = 3.9$. The energy flux being deposited into the thermal source is 1.5×10^{12} ergs cm^{-2} s^{-1} and the hard X-ray flux above 10 keV averaged over the 2.5 s life of the source is 3.2×10^8 ergs cm^{-2} s^{-1} which leads to an efficiency $\epsilon_T = 2.1 \times 10^{-4}$. An electron power-law energy distribution must have an index $\delta = \gamma + 1$ to produce the same spectrum by thick-target processes (Brown 1976). Using the formulae in Brown (1971) for the bremsstrahlung loss per second ΔE_B and the Coulomb loss per second ΔE_c due to electron-electron collisions, we find that the efficiency of a nonthermal thick-target source above an energy of E_1 is

$$\epsilon_{\rm NT} = 2.6 \times 10^{-7} \frac{\int_{E_1}^{\infty} \epsilon^{-\gamma} d\epsilon}{\int_{E_1}^{\infty} E^{-\delta} dE} . \tag{11}$$

With $E_1 = 10$ keV, $\gamma = 3.9$, and $\delta = 5$, $\epsilon_{\rm NT} = 3.5 \times 10^{-6}$ and the thermal source is 60 times more efficient. This efficiency gain is proportional to density so that again a thermal source offers any real gain only above $n = 10^{10}$ cm^{-3}. The reason that this gain is 2.4 times larger than in SL is that the comparison in SL was made with an electron of energy 41 keV, whereas here the comparison is made with a distribution of electrons with average energy 13.3 keV. As can be seen from equation (22) of SL, $\epsilon_{\rm NT}$ is proportional to the energy E, which explains the increase in efficiency in this paper. The comparison here is more meaningful, but could be made only after the spectrum was computed. The relatively good agreement on the efficiency of the thermal source here and in SL at the same density shows that despite the use of an artificial thermal conductivity, the basic results obtained there were correct.

Since arguments on the desirability of interacting the conduction front with the transition region and chromosphere, and on two-dimensional calculations were given in SL, we do not repeat them here. The main result of this paper is that there exists a natural conduction mode in which a thermal source leads to a power-law hard X-ray photon spectrum indistinguishable from nonthermal electron streaming models. The conditions for the presence of this mode are a sensitive function of the electron-ion thermal coupling. We have argued, in agreement with simulations, that the main effect of hot ions is to saturate the instability in the trapping stage and to take the energy lost by the electrons. To model this phenomenon and confirm these expectations would require an additional temperature equation for the hot ion tail. As noted by Manheimer (1977), this "does seem to be a fruitful area for future research." We can only reiterate this prognosis. In this connection it would also be valuable to know at what density a hot ion tail begins to affect the dispersion characteristics and hence the instability criteria for the ion-acoustic waves.

The authors are grateful to Dr. J. Boris for providing us with the flux-corrected transport algorithm and other advice, to Dr. G. Zimmerman for information on how flux limiters are applied in laser fusion, and to Drs. J. Brown and P. Hoyng for useful discussions. The work of D. F. S. was supported by NASA grant NSG-7507.

APPENDIX

COMPUTATIONAL SCHEME

We have symbolically the system

$$\frac{d\boldsymbol{S}}{dt} = D_1(\boldsymbol{S}) + D_2(\boldsymbol{S}) , \tag{A1}$$

where $\boldsymbol{S}$ is the variable vector for the system (3)–(6) and D_1 and D_2 are spatial operators. Equation (A1) can be replaced by the discrete analog

$$\boldsymbol{S}^{n+1} - \boldsymbol{S}^n = \Delta t[D_1(\boldsymbol{S}^n) + D_2(\boldsymbol{S}^{n+1})] , \tag{A2}$$

where the superscripts index the time steps of duration Δt. This system can be solved in two steps:

$$\boldsymbol{\sigma}^{n+1} = \boldsymbol{S}^n + \Delta t D_1(\boldsymbol{S}^n) , \tag{A3}$$

$$\boldsymbol{S}^{n+1} = \boldsymbol{\sigma}^{n+1} + \Delta t D_2(\boldsymbol{S}^{n+1}) , \tag{A4}$$

where equation (A3) defines $\boldsymbol{\sigma}$. Thus equations (3)–(6) were broken into the explicit equations (3)–(4), and

$$\frac{3}{2}\frac{\partial}{\partial t} nK\tilde{T}_e + \frac{3}{2}\frac{\partial}{\partial x} nK\tilde{T}_e v + nK\tilde{T}_e \frac{\partial v}{\partial x} = \frac{\partial \epsilon}{\partial t} , \qquad \frac{3}{2}\frac{\partial}{\partial t} nK\tilde{T}_i + \frac{3}{2}\frac{\partial}{\partial x} nK\tilde{T}_i v + nK\tilde{T}_i \frac{\partial v}{\partial x} = 0 , \tag{A5}$$

which were advanced using the explicit low phase error flux-corrected transport method of Boris and Book (1976) and the implicit equations

$$\frac{3}{2}\frac{\partial}{\partial t}nKT_e = -\frac{\partial Q}{\partial x} - \frac{3}{2}nK(T_e - T_i)f_{\rm eq} + R_L + C_{\rm te}, \qquad \frac{3}{2}\frac{\partial}{\partial t}nKT_i = \frac{3}{2}nK(T_e - T_i)f_{\rm eq} + C_{\rm ti}\,, \tag{A6}$$

which were solved for T_e and T_i by a completely implicit scheme holding other variables fixed. The tildes in equations (A5) indicate provisional values. In order to obtain second-order accuracy in time, equations (3), (4), (A5), and (A6) were advanced provisionally to $t^n + \frac{1}{2}\Delta t$, where the sources and velocity were evaluated, and then the advance to the full time step was made using the "centered" sources. The method conserved total energy to $\sim 0.2\%$.

REFERENCES

Boris, J. P., and Book, D. L. 1976, *Methods in Computational Physics*, Vol. **16** (New York: Academic), p. 85.
Brown, J. C. 1971, *Solar Phys.*, **18**, 849.
———. 1974, *IAU Symposium No. 57, Coronal Disturbances*, ed. G. Newkirk (Dordrecht: Reidel), p. 395.
———. 1976, *Phil. Trans. Roy. Soc. Lond. A*, **281**, 473.
Brown, J. C., Melrose, D. B., and Spicer, D. S. 1979, *Ap. J.*, **228**, 592 (BMS).
Caponi, M. Z., and Krall, N. A. 1975, *Phys. Fluids*, **18**, 699.
Crannell, C. J., Frost, K. J., Mätzler, C., Okki, K., and Saba, J. L. 1978, *Ap. J.*, **223**, 620.
Elcan, M. J. 1978, *Ap. J.*, **226**, L99.
Emslie, G. A., and Brown, J. C. 1980, *Ap. J.*, submitted.
Hoyng, P., Brown, J. C., and van Beek, H. F. 1976, *Solar Phys.*, **48**, 197.
Jordan, C. 1975, *IAU Symposium No. 68, Solar Gamma, X-, and EUV Radiation*, ed. S. R. Kane (Dordrecht: Reidel), p. 109.
Kane, S. R. 1974, *IAU Symposium No. 57, Coronal Disturbances*, ed. G. A. Newkirk (Dordrecht: Reidel), p. 105.
Manheimer, W. M. 1977, *Phys. Fluids*, **20**, 265.
Smith, D. F. 1980, *Solar Phys.*, in press.
Smith, D. F., and Lilliequist, C. G. 1979, *Ap. J.*, **232**, 582 (SL).
Stenzel, R. L., and Gekelman, W. 1978, *Phys. Fluids*, **21**, 2024.
Stringer, T. E. 1964, *J. Nucl. Energy C*, **6**, 267.
Tindo, I. P., Shuryghin, A. I., and Steffen, W. 1976, *Solar Phys.*, **46**, 219.
Wiehl, H. J., and Schöchlin, W. A. 1980, *IAU Symposium No. 86, Radio Physics of the Sun*, ed. M. R. Kundu and T. E. Gergely (Dordrecht: Reidel), in press.
Zeldovich, Ya. B., and Raizer, Yu. P. 1967, *Physics of Shock Waves and High-Temperature Hydrodynamic Phenomena*, Vol. **2** (New York: Academic Press).

LAWRENCE H. AUER: High Altitude Observatory, P.O. Box 3000, Boulder, CO 80307

DEAN F. SMITH: Department of Astro-Geophysics, Campus Box 391, University of Colorado, Boulder, CO 80309